JACS
JOURNAL OF THE AMERICAN CHEMICAL SOCIETY

Communication

pubs.acs.org/JACS

Organometal Halide Perovskite Solar Cell Materials Rationalized: Ultrafast Charge Generation, High and Microsecond-Long Balanced Mobilities, and Slow Recombination

Carlito S. Ponseca, Jr.,*[,†] Tom J. Savenije,[‖] Mohamed Abdellah,[†,‡] Kaibo Zheng,[†] Arkady Yartsev,[†] Tobjörn Pascher,[†] Tobias Harlang,[†] Pavel Chabera,[†] Tonu Pullerits,[†] Andrey Stepanov,[§] Jean-Pierre Wolf,[§] and Villy Sundström*[,†]

[†]Division of Chemical Physics, Lund University, Box 124, 221 00 Lund, Sweden

[‖]Department of Chemical Engineering, Delft University of Technology, 2628 BL Delft, The Netherlands

[§]GAP-Biophotonics, University of Geneva, 1211 Geneva 4, Switzerland

[‡]Department of Chemistry, Qena Faculty of Science, South Valley University, Qena 83523, Egypt

Supporting Information

ABSTRACT: Organometal halide perovskite-based solar cells have recently been reported to be highly efficient, giving an overall power conversion efficiency of up to 15%. However, much of the fundamental photophysical properties underlying this performance has remained unknown. Here, we apply photoluminescence, transient absorption, time-resolved terahertz and microwave conductivity measurements to determine the time scales of generation and recombination of charge carriers as well as their transport properties in solution-processed $CH_3NH_3PbI_3$ perovskite materials. We found that electron–hole pairs are generated almost instantaneously after photoexcitation and dissociate in 2 ps forming highly mobile charges (25 $cm^2\ V^{-1}\ s^{-1}$) in the neat perovskite and in perovskite/alumina blends; almost balanced electron and hole mobilities remain very high up to the microsecond time scale. When the perovskite is introduced into a TiO_2 mesoporous structure, electron injection from perovskite to the metal oxide is efficient in less than a picosecond, but the lower intrinsic electron mobility of TiO_2 leads to unbalanced charge transport. Microwave conductivity measurements showed that the decay of mobile charges is very slow in $CH_3NH_3PbI_3$, lasting up to tens of microseconds. These results unravel the remarkable intrinsic properties of $CH_3NH_3PbI_3$ perovskite material if used as light absorber and charge transport layer. Moreover, finding a metal oxide with higher electron mobility may further increase the performance of this class of solar cells.

A highly efficient solar cell material should absorb light over a wide spectral range, generate charges with high efficiency, and transport these photogenerated charges to the electrodes with minimum losses. Several groups have reported power conversion efficiencies (PCEs) from 10% to 15% for solution processed organometal halide perovskite (OMHP)-based solar cells in the past two years.[1−3] More recently, it was shown that these classes of materials have electron–hole diffusion lengths of at least 100 nm for triiodide absorber[4] and longer than 1 μm for trihalide OMHP.[5] However, the fundamental photophysical processes underlying solar cell function need to be understood in order to fully utilize the properties of these materials. For instance, it is not known whether the exceptionally long diffusion lengths are related to molecular excitons, i.e., tightly bound electron–hole pairs, or to highly mobile charge carriers. Hence, the nature of the initial photophysical product is not known. The exact role of the metal oxide TiO_2 as electron acceptor and charge transport layer in an OMHP-based photovoltaic cell is also not understood. Moreover, the influence of introducing OMHP in the open voids of sintered isolating nanoparticles (NPs), e.g. Al_2O_3 on the optoelectronic properties, has not yet been addressed. Therefore, a study on the charge carrier dynamics, including photogeneration and recombination is very much warranted but still lacking in the current literature.

In this work, a combination of spectroscopic techniques, namely photoluminescence (PL), transient absorption (TA), time-resolved terahertz spectroscopy (TRTS), and time-resolved microwave conductivity (TRMC) were used to monitor the light-induced processes from the subpicosecond to a hundred of microsecond time scale. We should stress that both TRTS and TRMC have been demonstrated as powerful techniques for studying charge carrier dynamics and the mobility in different organic and inorganic systems.[6−12] Neat methylammonium lead iodide ($CH_3NH_3PbI_3$) was prepared to elucidate the intrinsic transport properties of the OMHP, while $CH_3NH_3PbI_3$ on Al_2O_3 was studied to resolve the influence of the nanostructure on the charge carrier dynamics. To clarify the role of an electron-accepting metal oxide on the dynamics of excited states in the perovskite, samples with $CH_3NH_3PbI_3$ introduced in TiO_2 NPs were also prepared. The importance and complexity of different material contacts, their heterogeneity, and differences in the morphology for the charge carrier dynamics were pointed out in ref 13. Here we focus on the carrier dynamics in neat $CH_3NH_3PbI_3$ and when a layer of mesoporous NPs TiO_2 and Al_2O_3 is filled with OMHP.

Received: December 11, 2013
Published: March 21, 2014

   dx.doi.org/10.1021/ja412583t | J. Am. Chem. Soc. 2014, 136, 5189−5192

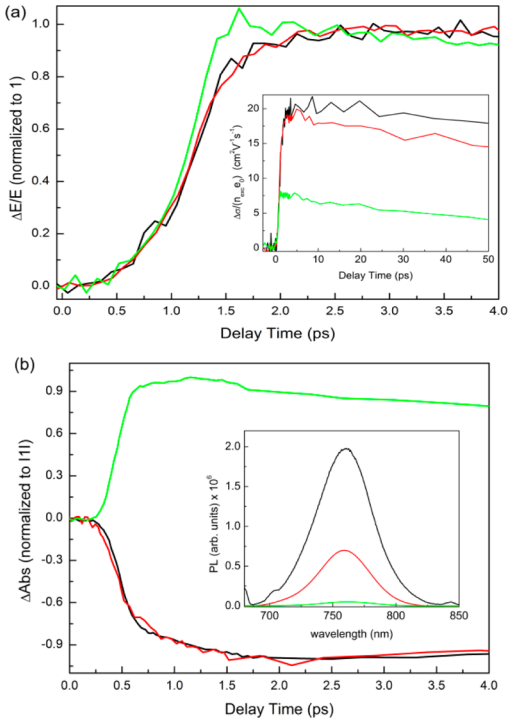

Figure 1. Early time dynamics of neat $CH_3NH_3PbI_3$ (black), $CH_3NH_3PbI_3/Al_2O_3$ (red), and $CH_3NH_3PbI_3/TiO_2$ (green). (a) THz kinetics (λ_{pump} = 400 nm, $I_{exc} = 1.7 \times 10^{13}$ ph/cm^2 per pulse) normalized to |1|. Inset is the THz photoconductivity kinetics for the first 50 ps normalized with $n_{exc}e$. (b) TA kinetics (λ_{pump} = 603 nm, λ_{probe} = 970 nm, $I_{exc} = 6.0 \times 10^{14}$ ph/cm^2 per pulse). Inset is the corresponding PL spectra (λ_{pump} = 550 nm).

The early time THz kinetics of neat $CH_3NH_3PbI_3$, $CH_3NH_3PbI_3/Al_2O_3$, and $CH_3NH_3PbI_3/TiO_2$ are shown in Figure 1a. For neat $CH_3NH_3PbI_3$ and $CH_3NH_3PbI_3/Al_2O_3$, an instrument limited rise (A = 70%) assigned to generation of electron–hole pairs is followed by a second (~2 ps, A = 30%) rise before reaching its maximum. Upon photoexcitation, electron–hole pairs are initially Coulombically bound and require an activation energy on the order of the thermal energy, kT, to dissociate into mobile charges. This dissociation could take a few ps and in this case manifested as the ~2 ps rise in the THz kinetics of neat $CH_3NH_3PbI_3$ and $CH_3NH_3PbI_3/Al_2O_3$. For $CH_3NH_3PbI_3/TiO_2$, the THz transient rises faster than in the other two samples and grows with a response-limited rise time. We previously showed that in the presence of a metal oxide with a high electron affinity, electron injection from a photoexcited sensitizer to the oxide can be ultrafast, e.g., in CdSe quantum dot sensitized ZnO[8] and dye sensitized TiO_2.[12] We therefore assign the response limited rise in THz photoconductivity for $CH_3NH_3PbI_3/TiO_2$ as subps electron injection from the OMHP to TiO_2. Moreover, the transient THz photoconductivity kinetics (Figure 1a inset), normalized with excitation density, shows that the charge mobility of $CH_3NH_3PbI_3/TiO_2$ is ~7.5 cm^2 V^{-1} s^{-1}, ~3–4 times lower than in neat $CH_3NH_3PbI_3$ and the $CH_3NH_3PbI_3/Al_2O_3$ (i.e., ~20 cm^2 V^{-1} s^{-1}), supporting the proposal that electron injection occurs in $CH_3NH_3PbI_3/TiO_2$.

Optical TA kinetics of neat $CH_3NH_3PbI_3$ and $CH_3NH_3PbI_3/Al_2O_3$ is shown in Figure 1b. It is characterized by an instrument limited negative response followed by an ~2 ps of further decrease. The time scale of this two component signal is consistent with the two step rise in THz kinetics confirming that

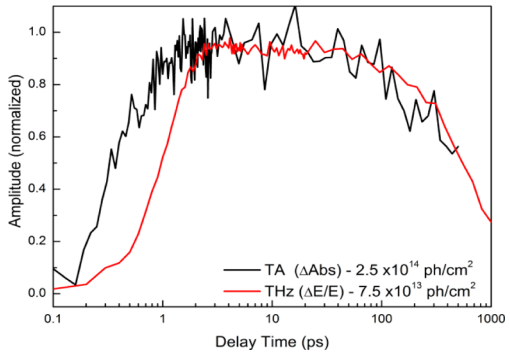

Figure 2. Comparison TA and TRTS kinetics for neat $CH_3NH_3PbI_3$ showing that THz mobility remains constant for at least 1 ns.

charges are not instantaneously created. Furthermore, the negative signal, in a wavelength region lacking ground-state absorption, is a characteristic of stimulated emission, which agrees with the steady-state PL spectra (Figure 1b inset) showing radiative recombination. In contrast, a single component ultrafast rise with positive sign manifests in the kinetics of $CH_3NH_3PbI_3/TiO_2$. This is consistent with the time scale of the appearance of electrons in TiO_2[1,14] and identical to the rise time of the THz kinetics (Figure 1a). Although not complete, strong quenching of the PL in $CH_3NH_3PbI_3/TiO_2$ is additional evidence for electron injection. A scanning electron microscope image (Figure S1C) of $CH_3NH_3PbI_3/TiO_2$ shows no evidence of domains of $CH_3NH_3PbI_3$ larger than 500 nm, which means that the mesoporous network of $CH_3NH_3PbI_3$ is formed within TiO_2 NPs similar to that presented in ref 1. However, smaller domains of $CH_3NH_3PbI_3$ may also be present due to voids that may have been created by the TiO_2 NPs, but their contribution is relatively small, as evidenced by the strong PL quenching and the ultrafast rise in THz kinetics indicating that electron injection is still very efficient.

THz photoconductivity kinetics on tens of ps time scale, for all three studied materials, exhibit a slow decay as shown in the inset of Figure 1a. Since the THz response is a product of carrier concentration and mobility, it is not possible to conclude, based on the THz kinetics alone, if this decay is due to decrease of charge concentration (i.e., charge recombination) or to relaxation of carrier mobility with time. Optical TA on the other hand is a direct measure of the carrier concentration. In Figure 2 kinetics of neat $CH_3NH_3PbI_3$ was measured with TA and TRTS at similar intensities (~10^{13} ph/cm^2 per pulse). Within the experimental error, we found that they are identical, implying that carrier mobility has to remain constant for at least 1 ns, otherwise a faster decay of the THz kinetics would be observed. Consequently, this means that the decay of the THz conductivity is a result of a decreasing carrier concentration (nongeminate recombination, see below). The dependence of the THz decay on the excitation density is also illustrated in Figure S2, wherein at the lowest excitation intensity (2.0×10^{12} ph/cm^2 per pulse) there is no decay observed for the first 200 ps where the charge carrier mobility is found to be highest, i.e., 25 cm^2 V^{-1} s^{-1}. We note that this remarkably high THz mobility in solution processed OMHP is similar with the mobility recently obtained by Wehrenfennig et al.[15]

THz photoconductivity spectra were also measured 10 ps after photoexcitation (Figure 3). Within experimental error, both the amplitude and shape of the spectra of neat $CH_3NH_3PbI_3$ and $CH_3NH_3PbI_3/Al_2O_3$ are the identical. However, for

dx.doi.org/10.1021/ja412583t | J. Am. Chem. Soc. 2014, 136, 5189–5192

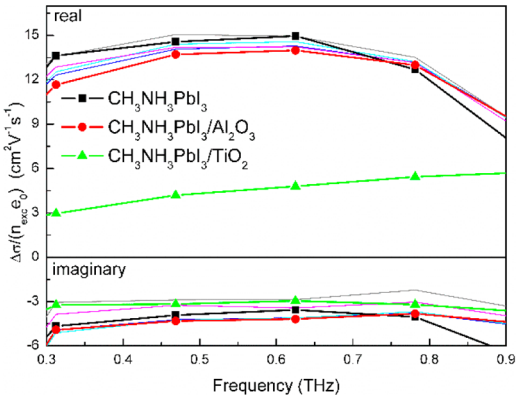

Figure 3. THz photoconductivity spectra measured 10 ps (trace with symbols) after photoexcitation and normalized with $n_{exc}e$. Solid traces are THz photoconductivity spectra of $CH_3NH_3PbI_3/Al_2O_3$ at different pump probe delays (blue 100 ps, cyan 200 ps, magenta 600 ps, gray 950 ps).

$CH_3NH_3PbI_3/TiO_2$, the spectral shape is qualitatively different, and the signal size is approximately four times lower than for $CH_3NH_3PbI_3$ and $CH_3NH_3PbI_3/Al_2O_3$ (as also shown in the THz kinetics of Figure 1a, inset). From the above observations we can draw a number of conclusions: First, the identical THz spectra and photoconductivity kinetics of neat $CH_3NH_3PbI_3$ and $CH_3NH_3PbI_3/Al_2O_3$ show that the presence of Al_2O_3 does not alter the dynamics and mobility of the charges in the OMHP, on the distance scale probed by the THz measurements (<100 nm). Second, the presence of TiO_2 NPs accelerates formation of charge carriers, which leads to efficient electron injection in <1 ps due to favorable band energy alignment of TiO_2 and the OMHP. However, due to the low intrinsic mobility of TiO_2,[16] injection leads to unbalanced transport of charges (see below), lowering the overall mobility. We also show in Figure 3 that the THz photoconductivity spectra (normalized with excitation and decay due to nongeminate recombination) at different pump probe delay times (100–950 ps) are identical, supporting our assertion that mobility remains high up to at least 1 ns.

Unbalanced electron and hole mobilities, which are orders of magnitude different in bulk heterojunction solar cells, result in space charge-limited photocurrents lowering the PCE.[17] Therefore it is important to assess the mobilities of both electrons and holes. A THz measurement on only one material does not provide this information, but by comparing several materials with known electron or hole mobilities this quantity can be derived. From the THz measurements of porous TiO_2 films, it was shown that its intrinsic electron mobility is $\ll 1$ cm^2 V^{-1} s^{-1}.[9,11,16] In this case, electron mobility of TiO_2 in $CH_3NH_3PbI_3/TiO_2$ should be the same, i.e., the THz response is mainly due to the holes in the OMHP phase having a mobility of close to 7.5 cm^2 V^{-1} s^{-1}. Consequently, from the measured THz mobility of ~20 cm^2 V^{-1} s^{-1} for $CH_3NH_3PbI_3$ and $CH_3NH_3PbI_3/Al_2O_3$, we can conclude that electron mobility in the perovskite phase is ~12.5 cm^2 V^{-1} s^{-1}. The $12.5/7.5 \approx 2$ ratio of electron and hole mobilities in the OMHP phase is in agreement with the recent theoretical calculations of the relative effective masses of electrons and holes.[18] The finding that electron and hole mobility is almost balanced is novel key information for the understanding why OMHP-only or OMHP/Al_2O_3 solar cells are so efficient.

Slow electron–hole recombination and persistent high mobility are essential features for an efficient solar cell. By using the TRMC technique, we monitor the changes in

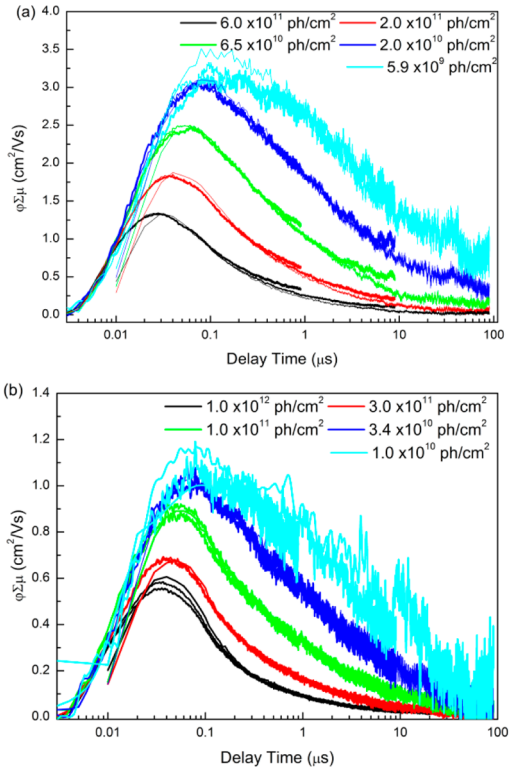

Figure 4. TRMC kinetics of (a) $CH_3NH_3PbI_3/Al_2O_3$ and (b) $CH_3NH_3PbI_3/TiO_2$ at different excitation densities measured up to 100 μs.

photoconductance up to a hundred of microseconds at very low excitation density (carrier density), minimizing the contribution of nongeminate recombination, and allowing characterization of even very slow recombination dynamics. Figure 4a,b shows TRMC kinetics of $CH_3NH_3PbI_3/Al_2O_3$ and $CH_3NH_3PbI_3/TiO_2$, respectively, measured over two orders of excitation fluence (5.9×10^9–6×10^{11} ph/cm^2 per pulse) and up to 100 μs. All transients exhibit a nonexponential decay with a fast (~100 ns) initial part—faster at higher intensity—and a slow microsecond tail with increasing lifetime and amplitude for lower intensity, a characteristic behavior for nongeminate charge recombination.[19,20] The high mobility of electrons and holes in the OMHP phase allows rapid diffusion away from their locus of generation, effectively retarding geminate recombination. The consequence of this is intensity-dependent TRMC kinetics dominated by nongeminate electron–hole recombination. The TRMC kinetics measured down to the lowest intensity shows that geminate recombination must be very slow, at least tens of microseconds (Figure 4a,b). However, since the TRMC response is a product of carrier concentration and mobility, just as in TRTS, it is not possible to extract from a single transient the precise contribution of charge carrier recombination and carrier relaxation to the observed TRMC decay. Nevertheless, at the lowest excitation intensity (5.9×10^9 ph/cm^2 per pulse) the decay of the TRMC kinetics occurs on a 1 μs time scale and longer, showing that geminate and nongeminate recombination as well as charge carrier relaxation (i.e., time dependence of mobility) must all be considerably slower than 1 μs. The most important conclusion from these results is that electron–hole recombination is very slow under ambient sunlight, tens of μs time scale, and high carrier mobility also extends up to the microsecond time scale. We discussed above the contribution of

dx.doi.org/10.1021/ja412583t | J. Am. Chem. Soc. 2014, 136, 5189–5192

electron and hole in the THz mobilities in the perovskite phase and concluded that electrons are twice as mobile as the holes. Assuming that the same ratio holds at the microsecond time scale, the sum of mobilities of electrons and holes at this frequency is 3 $cm^2\ V^{-1}\ s^{-1}$, in both neat $CH_3NH_3PbI_3$ and $CH_3NH_3PbI_3/Al_2O_3$ (Figure 4a) leads to the conclusion that the electron mobility is 2 $cm^2\ V^{-1}\ s^{-1}$, while the hole mobility is 1 $cm^2\ V^{-1}\ s^{-1}$. This in turn means that the measured TRMC mobility of 1 $cm^2\ V^{-1}\ s^{-1}$ in $CH_3NH_3PbI_3/TiO_2$ originates from the mobile holes in the perovskite phase; electron mobility is therefore much lower in TiO_2 than in $CH_3NH_3PbI_3$ in line with previous TRMC measurements.[10,11]

By combining the results of TRTS, TRMC, and TA, we can now paint a picture of the carrier dynamics in all three studied samples, covering the time scale from less than a picosecond to hundreds of microseconds and over a very wide range of carrier densities. At high carrier density (10^{13}–10^{14} ph/cm^2 per pulse) achieved in the TRTS and TA measurements (Figures 1, 2, S2) extensive electron–hole nongeminate recombination leads to charge quenching and decay of photoconductivity signal and absorption on the picosecond to several hundred picosecond time scale. From the measurement of TRTS kinetics at low intensity (~10^{12} ph/cm^2 per pulse; Figure S2) and comparison with TA kinetics (Figure 2), a maximum mobility of ~25 $cm^2\ V^{-1}\ s^{-1}$ was concluded to last for at least 1 ns, for neat $CH_3NH_3PbI_3$ and $CH_3NH_3PbI_3/Al_2O$. With the TRMC measurements we can reach much lower excitation intensities and carrier densities, such that the rate and impact of nongeminate recombination on the dynamics becomes progressively slower and less pronounced (Figure 4). At the lowest carrier density achieved (5.9×10^9 ph/cm^2 per pulse, Figures 4, S3), there is almost no decay of the microwave conductivity over 1 μs, showing that decay of carrier mobility as well as carrier population occurs on a >1 μs time scale, and microwave mobility exceeding 3 $cm^2\ V^{-1}\ s^{-1}$ may extend to the microsecond time scale in neat $CH_3NH_3PbI_3$ and $CH_3NH_3PbI_3/Al_2O_3$. The fact that nongeminate recombination persists down to very low carrier densities is another signature of charge motion over large distances. In $CH_3NH_3PbI_3/TiO_2$ the peak mobility is lower by approximately a factor of 4 as a result of electron injection to TiO_2.

Our findings show that neat perovskite and perovskite/Al_2O_3 have several nearly ideal solar cell properties: highly mobile electron and holes are formed within a few picoseconds, and mobilities of both are almost balanced and remain high to microseconds time scale. Very slow microsecond time scale recombination at ambient solar intensities in combination with high and almost equal electron and hole mobilities guarantees very efficient charge collection and thus high solar cell efficiency. The results also show that, as a consequence of electron injection from the perovskite to the TiO_2 with very low electron mobility, overall mobility is lowered. We note also that the lower Fermi level of TiO_2 decreases the open circuit voltage leading to lower overall efficiency. A possible improvement of solar cell performance would be to engineer the active materials such that both electron and hole mobilities are on the level of the electron mobility in the perovskite.

■ ASSOCIATED CONTENT

Supporting Information

Experimental details and SEM images. This information is available free of charge via the Internet at http://pubs.acs.org.

■ AUTHOR INFORMATION

Corresponding Authors

carlito.ponseca@chemphys.lu.se
villy.sundstrom@chemphys.lu.se

Notes

The authors declare no competing financial interest.

■ ACKNOWLEDGMENTS

The Swedish Energy Agency (STEM), the Swedish Research Council, the Knut and Alice Wallenberg foundation, and the European Research Council (Advanced Investigator Grant to V.S., 226136-VISCHEM) are acknowledged. The nanometer Consortium at Lund University (nmc@LU) is also acknowledged.

■ REFERENCES

(1) Lee, M. M.; Teuscher, J.; Miyasaka, T.; Murakami, T. N.; Snaith, H. J. *Science* **2012**, *338*, 643.
(2) Heo, J. H.; Im, S. H.; Noh, J. H.; Mandal, T. N.; Lim, C.-S.; Chang, J. A.; Lee, Y. H.; Kim, H. J.; Sarkar, A.; Nazeeruddin, M. K.; Grätzel, M.; Seok, S. I. *Nat. Photonics* **2013**, *7*, 486.
(3) Burschka, J.; Pellet, N.; Moon, S. J.; Humphry-Baker, R.; Gao, P.; Nazeeruddin, M. K.; Grätzel, M. *Nature* **2013**, *499*, 316.
(4) Xing, G.; Mathews, N.; Sun, S.; Lim, S. S.; Lam, Y. M.; Grätzel, M.; Mhaisalkar, S.; Sum, T. C. *Science* **2013**, *342*, 344.
(5) Stranks, S. D.; Eperon, G. E.; Grancini, G.; Menelaou, C.; Alcocer, M. J. P.; Leijtens, T.; Herz, L. M.; Petrozza, A.; Snaith, H. J. *Science* **2013**, *342*, 341.
(6) Ponseca, C. S., Jr.; Yartsev, A.; Wang, E.; Andersson, M.; Vithanage, D.; Sundström, V. *J. Am. Chem. Soc.* **2012**, *134*, 11836.
(7) Ponseca, C. S., Jr.; Němec, H.; Vukmirović, N.; Fusco, S.; Wang, E.; Andersson, M.; Chavera, P.; Yartsev, A.; Sundström, V. *J. Phys. Chem. Lett.* **2012**, *3*, 2442.
(8) Zidek, K.; Zheng, K.; Ponseca, C. S., Jr.; Messing, M. E.; Wallenberg, L. R.; Chabera, P.; Abdellah, M.; Sundström, V.; Pullerits, T. *J. Am. Chem. Soc.* **2012**, *134*, 12110.
(9) Savenije, T. J.; Huijser, A.; Vermeulen, M. J. W.; Katoh, R. *Chem. Phys. Lett.* **2008**, *461*, 93.
(10) Murthy, D. H. K.; Gao, K.; Vermeulen, M. J. W.; Siebbeles, L. D. A.; Savenije, T. J. *J. Phys. Chem. C* **2012**, *116*, 9214.
(11) Fravventura, M. C.; Deligiannis, D.; Schins, J. M.; Siebbeles, L. D. A.; Savenije, T. J. *J. Phys. Chem. C* **2013**, *117*, 8032.
(12) Němec, H.; Rochford, J.; Taratula, O.; Galoppini, E.; Kužel, P.; Polívka, T.; Yartsev, A.; Sundström, V. *Phys. Rev. Lett.* **2010**, *104*, 197401.
(13) Marchioro, A.; Teuscher, J.; Friedrich, D.; Kunst, M.; van de Krol, R.; Moehl, T.; Grätzel, M.; Moser, J.-E. *Nature Photon.* **2014**, *8*, 250.
(14) Rothenberger, G.; Fitzmaurice, D.; Grätzel, M. *J. Phys. Chem.* **1992**, *96*, 5983.
(15) Wehrenfennig, C.; Eperon, G. E.; Johnston, M. B.; Snaith, S. J.; Herz, L. M. *Adv. Mater.* **2013**, DOI: 10.1002/adma.201305172.
(16) Hendry, E.; Koeberg, M.; O'Regan, B.; Bonn, M. *Nano Lett.* **2006**, *6*, 755.
(17) Blom, P. W. M.; Mihailetchi, V. D.; Koster, L. J. A.; Markov, D. E. *Adv. Mater.* **2007**, *19*, 1551.
(18) Umari P.; Mosconi, E.; Angelis, F. D. 2013 arXiv:1309.4895.
(19) De, S.; Pascher, T.; Maiti, M.; Jespersen, K. G.; Kesti, T.; Zhang, F.; Inganas, O.; Yartsev, A.; Sundstrom, V. *J. Am. Chem. Soc.* **2007**, *129*, 8466.
(20) Pal, S. K.; Kesti, T.; Maiti, M.; Zhang, F.; Inganäs, O.; Hesllström, S.; Andersson, M. R.; Oswald, F.; Langa, F.; Österman, T.; Pascher, T.; Yartsev, A.; Sundström, V. *J. Am. Chem. Soc.* **2010**, *132*, 12440.